PHYSICAL REVIEW E VOLUME 50, NUMBER 2 AUGUST 1994

Oscillations, complex spatiotemporal behavior, and information transport in networks of excitatory and inhibitory neurons

Alain Destexhe*
Université Libre de Bruxelles, Code Postal 231, Campus Plaine, Boulevard du Triomphe, B-1050 Bruxelles, Belgium
(Received 25 February 1994)

Various types of spatiotemporal behavior are described for two-dimensional networks of excitatory and inhibitory neurons with time delayed interactions. It is described how the network behaves as several structural parameters are varied, such as the number of neurons, the connectivity, and the values of synaptic weights. A transition from spatially uniform oscillations to spatiotemporal chaos via intermittentlike behavior is observed. The properties of spatiotemporally chaotic solutions are investigated by evaluating the largest positive Lyapunov exponent and the loss of correlation with distance. Finally, properties of information transport are evaluated during uniform oscillations and spatiotemporal chaos. It is shown that the diffusion coefficient increases significantly in the spatiotemporal phase similar to the increase of transport coefficients at the onset of fluid turbulence. It is proposed that such a property should be seen in other media, such as chemical turbulence or networks of oscillators. The possibility of measuring information transport from appropriate experiments is also discussed.

PACS number(s): 87.10.+e, 87.22.−q, 05.45.+b, 47.27.Eq

INTRODUCTION

Neurons of the cerebral cortex are characterized by a marked tendency to participate in coherent oscillatory behavior of various frequencies. Oscillations in the 30–60 Hz range can be seen in relation to the processing of sensory information (reviewed in [1]), delta (0.5–4 Hz) and spindle (7–14 Hz) oscillations are mostly seen during slow-wave sleep [2]. Measurements of the global activity of the brain, such as the field potentials or electroencephalograms, display indisputable periodicities but are nevertheless characterized by a high variability. In some cases, these global variables were shown to have very similar statistical and geometrical properties as deterministic chaos [3–6].

At the cellular level, trains of spikes produced by cortical neurons can be recorded extracellularly in awake animals, and show a considerable amount of variability (see Ref. [7] and references therein). These trains of spikes are usually analyzed as stochastic processes. During sleep, as more synchronized oscillatory activity sets in, the activity of single cortical neurons becomes more phasic, but is still characterized by a high variability [8].

The mechanisms that are thought to generate oscillatory activity are twofold. First, oscillations can be generated as an intrinsic property of the neurons. Most of central neurons are characterized by a set of voltage-dependent conductances that confer to the cells very complex properties of electroresponsiveness, including bursts of spikes and sustained oscillations (reviewed in [9,10]). It is now largely admitted that the origin of at least some of the oscillatory phenomena seen in the cortex cannot be dissociated from these intrinsic cellular properties [10]. Several models were proposed to account for oscillatory behavior from the interaction between neurons endowed with complex intrinsic properties (see for example Refs. [11,12]).

Second, coherent oscillations were also shown to depend highly on the presence of synaptic connections [10,13], as they can disappear if synaptic interactions are blocked by pharmacological means (see for example Ref. [14]). In models, coherent oscillations can also arise as collective property of a network of neurons in which individual units do not display intrinsic properties other than conventional excitability [15–20]. In this case, oscillations arise from the interplay of excitatory and inhibitory feedback provided by synaptic connections.

In this paper, we examine oscillatory phenomena of the latter kind. The particular case of isotropic networks of excitatory and inhibitory neurons is considered and is shown to generate a variety of oscillatory and complex spatiotemporal phenomena. Several properties of spatiotemporal chaos are shown to be qualitatively similar to turbulence in other isotropic media and possible experimental applications are discussed.

In Sec. I, the equations and the architecture of the network are defined; in Sec. II, the various types of spatiotemporal dynamics are described; in Sec. III, various methods are applied to characterize spatiotemporally chaotic phenomena.

I. ARCHITECTURE OF THE NETWORK

If the neuron is described by a single compartment containing a passive (leak) current and several synapses converging onto it, then a network of N excitatory and M inhibitory of such neurons can be described by

*Present address: The Salk Institute, Computational Neurobiology Laboratory, 10010 North Torrey Pines Road, La Jolla, CA 92037. FAX: (619) 587-0417. Electronic address: alain@salk.edu

$$C_m \frac{dX_i}{dt} = -g_L\,(X_i - V_L) - \sum_k g_{ki}^{EE}\,(X_i - V_E) - \sum_l g_{li}^{IE}\,(X_i - V_I),$$
$$C_m \frac{dY_j}{dt} = -g_L\,(Y_j - V_L) - \sum_k g_{kj}^{EI}\,(Y_j - V_E) - \sum_l g_{lj}^{II}\,(Y_j - V_I), \tag{1}$$
$$i,k = 1,...,N \quad , \quad j,l = 1,...,M,$$

where X_i and Y_j represent the membrane potential of excitatory and of inhibitory neurons, respectively, $C_m = 1$ μF/cm^2 is the specific membrane capacitance, $g_L = 0.25$ mS/cm^2 is the leakage conductance, and $V_L = -60$ mV is the leakage potential. The values chosen here are typical values of the neuronal membrane (see Ref. [21]). g_{ki}^{EE}, g_{li}^{IE}, g_{kj}^{EI}, and g_{lj}^{II} are the synaptic conductances for excitatory-to-excitatory (EE), inhibitory-to-excitatory (IE), excitatory-to-inhibitory (EI), and inhibitory-to-inhibitory (II) interactions. $V_E = 50$ mV and $V_I = -80$ mV are the equilibrium potentials for synaptic excitation and inhibition.

Synaptic interactions are described by using a sigmoid-type function for expressing the synaptic conductance as a function of the presynaptic membrane potential:

$$g_{ki} = \text{const} \times F(X_k(t-\tau)),$$
$$F(X) = \frac{1}{1+\exp[-(X+25)/5]}, \tag{2}$$

where X_k is the potential of the presynaptic neuron and $\tau = 2$ ms is the time delay due to signal propagation and synaptic transmission. This sigmoid function F gives the output activity of the neuron in function of its potential X. For the most negative values of the potential, the neuron is silent and $F \simeq 0$. Above a threshold value of $V \simeq -50$ mV, the output activity of the neuron increases and saturates to a maximum value of $F \simeq 1$ for higher potentials. Such a sigmoid type of synaptic interaction is commonly used in neural network models [16,18,22].

Assuming the identity of all synaptic conductances of the same type (e.g., EE, IE, EI, or II), leads to the following set of equations:

$$\frac{dX_i}{dt} = -\gamma\,(X_i - V_L) - (X_i - V_E)\,\omega_1 \sum_k F(X_k(t-\tau_{ki})) - (X_i - V_I)\,\omega_2 \sum_l F(Y_l(t-\tau_{li})),$$
$$\frac{dY_j}{dt} = -\gamma\,(Y_j - V_L) - (Y_j - V_E)\,\omega_3 \sum_k F(X_k(t-\tau_{kj})) - (Y_j - V_I)\,\omega_4 \sum_l F(Y_l(t-\tau_{lj})), \tag{3}$$
$$i = 1,...,N, \quad j = 1,...,M,$$

where the conductances have been renormalized by C_m, which leads to the following set of parameters (in ms^{-1}): $\gamma = g_L/C_m$, $\omega_1 = g_{EE}/C_m$, $\omega_2 = g_{IE}/C_m$, $\omega_3 = g_{EI}/C_m$, and $\omega_4 = g_{II}/C_m$. The time delays τ_{ij} depend on the distance between the two neurons (see below). The sums run over the presynaptic neurons connected to each cell. This system is a generalization of models introduced previously [16,18,23–25].

Following the proportion of excitatory and inhibitory neurons, different schemes of connectivity can be considered. In this paper, we restricted our study to simple networks with uniform properties. The neurons are on a regular two-dimensional lattice and the connectivity is the same for each neuron. Connections are made *locally*, i.e., any given neuron connects all neurons laying within some neighborhood around itself. This type of connectivity has some analogies with the connectivity of the cerebral cortex for which neurons usually give numerous axon collaterals within some distance around them [26].

Two types of architecture are considered here and are shown in Fig. 1. Type 1 connectivity [Fig. 1(a)] corresponds to a network of N excitatory and N inhibitory cells, constituted of pairs of interconnected excitatory and inhibitory cells with connections between excitatory cells which may extend over longer distances. This type of connectivity was already considered in a previous study [25]. Type 2 connectivity [Fig. 1(b)] considers a different spatial arrangement of cells, specific to architectures where the proportion of excitatory and inhibitory cells mimics that of the cerebral cortex, which was found of about 75%–25% [27].

The connectivity is defined using a Hamming metric on the network. The distance between two neurons is counted as the sum of the difference between their coordinates. The time delay was chosen proportional to this distance. For a distance of 1 between neurons i and j, $\tau_{ij} = 2$ ms; for a distance of 2, $\tau_{ij} = 4$ ms, etc.

In this paper, the two mostly used connection patterns are the *nearest-neighbor* and the *secondary-neighbor* conditions. In the first case, every cell is connected to its nearest neighbors, as illustrated in Fig. 1. This corresponds to the set of connections of maximal distance equals to unity. In the case of secondary neighbor, every cell is connected to its nearest neighbors, plus the nearest

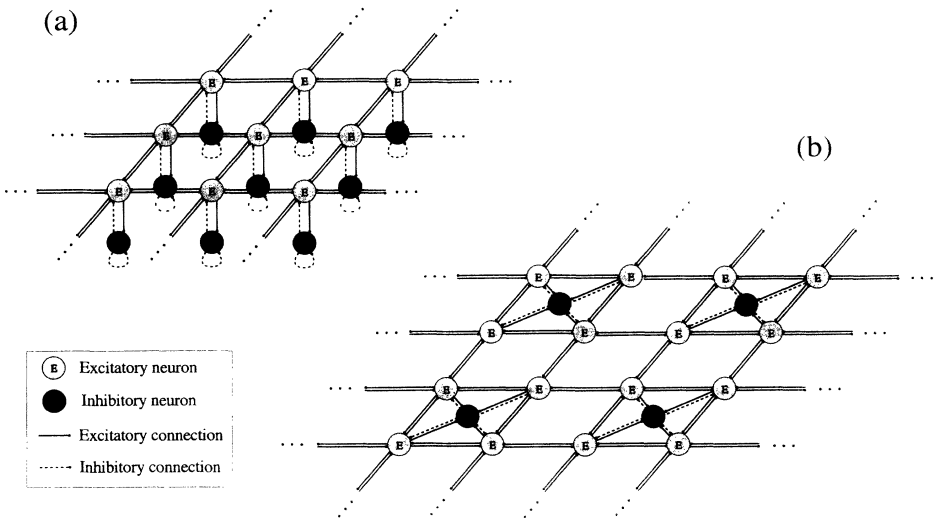

FIG. 1. Two different types of architecture of a network of excitatory and inhibitory neurons. For each type of architecture a few neurons are represented to illustrate the connectivity. Neurons are symbolized by shaded circles and connections by straight lines (see legend). (a) Type 1 connectivity. The network consists of a series of pairs of excitatory and inhibitory neurons arranged on a two-dimensional lattice. Connections between adjacent pairs are made between excitatory neurons only. (b) Type 2 connectivity. Excitatory and inhibitory neurons are in the ratio of 75% to 25%, and are equally distributed on the two dimensional network. For each type of architecture, only nearest-neighbor connections have been represented for simplicity.

neighbors of these, leading to a more extended pattern of connectivity including connections over one and two units of distance.

The boundary conditions of the network are chosen such that each neuron of the border has an equivalent connectivity as every other neuron in the network. The first type of such conditions is *periodic boundaries*, in which cells on the border connect those of the opposite border. Another possibility is to reflect the connection back in the network. According to such *reflective boundaries*, a connection to a neuron that lies outside the network is instead connected to the mirror image of that neuron in the network. In the case of nearest-neighbor connectivity, these conditions are equivalent to null flux conditions. Although both types of boundary conditions gave very similar results [28], only the latter are considered in the following.

The dynamical behavior of systems described by Eq. (3) was found to be essentially dependent on the number of neurons, the connectivity pattern, and the values of the synaptic weights. In the following section, the effect of some these parameters is described. In all cases, numerical simulations showed that the behavior of the network was remarkably robust to changes in the values of the other parameters, including the time delay (see also Refs. [24,25]).

Numerical integration of the equations was done using a Runge-Kutta algorithm with constant time steps, modified for delay differential equations. The values of the stationary states, the positions of the bifurcations, and the stability of the uniform periodic oscillations as obtained from stability analysis were always verified numerically. This is an important check, not only for the stability analysis, but also for the numerical integration of delay differential equations, which can be unstable, or give rise to long transients. Numerical simulations were always found to coincide perfectly with the results of the stability analysis of both fixed points and the uniform periodic oscillation [25,28].

II. SPATIOTEMPORAL DYNAMICS

The dynamical behavior of networks described by Eq. (3) are essentially dependent on the total number of neurons, on how they connect themselves, and on the value of the coupling between them. In this section, the dynamical behavior of Type 1 and Type 2 networks is described, for different sizes and different values of the excitatory-to-excitatory synaptic weight, Ω_1. The sequence of dynamical behavior presented here is representative of both Type 1 and Type 2 networks.

A. Resting stationary state

Synaptic interactions typically have a threshold. There exists a region of the membrane potential for which the coupling between cells is close to zero. Such a region is typically around the resting membrane potential, V_L. As $F(V_L) \simeq 0$, the uniform resting state $\{X_i \simeq V_L, Y_j \simeq V_L\}$ is usually a stable equilibrium.

However, such a stationary state may become unstable, partly because of the presence of the time delay and for sufficiently large values of synaptic weights [16]. In a

previous paper [24], it was shown that a simple system of two interconnected neurons, described by the same delay equations as Eq. (3) with $N = M = 1$, displays multistability and limit cycle oscillations. For large values of synaptic weights, it was found that the resting stationary state becomes unstable at some critical value Ω_1^H through a Hopf bifurcation. The limit cycle can also lose stability (at critical point Ω_1^E). For $\Omega_1 > \Omega_1^E$, both neurons were shown to be in a tonic stable stationary state, in which both cells are close to maximal activation.

The same solutions exist in the network if the conditions of connectivity are uniform, which is the case here. Equations (3) admit uniform solutions which are independent of the size of the system. On the other hand, the stability of these uniform solutions is not necessarily independent of the size of the system [25]. For fixed points, a stability analysis [29] showed that the stability of fixed points is independent of the size of the system.

Therefore, the typical equilibrium behavior of the system as a function of Ω_1 is as follows: a resting stationary state which is stable for small values of Ω_1 ($\Omega_1 < \Omega_1^H$) and a tonic stationary state which is stable for the highest values of Ω_1 ($\Omega_1 > \Omega_1^E$). In between these two stationary states, there exists a range of Ω_1 for which dynamical solutions can appear. These dynamical solutions are described in the following sections.

B. Uniform periodic oscillations

In a previous paper [25], it was shown that Eqs. (3) admit spatially uniform periodic solutions in which stability depends on the size of the network. As outlined above, these periodic oscillations arise following the destabilization of the uniform resting stationary state through a Hopf bifurcation. This type of oscillation is characterized by a perfect synchrony between neurons (Fig. 2).

For Type 1 connectivity, the stability of this uniform periodic solution was investigated by using a discretization method [25]. The system was linearized around the periodic solution, and discretized such as to obtain a mapping of the system over one period of the oscillation. The eigenvalues of the corresponding matrix are shown in Fig. 3. It was shown that the uniform periodic solution is stable only for small systems of neurons ($N \leq 9$). For larger sizes, the stability analysis shows that uniform periodic solution loses stability. Numerical simulations [25] confirmed this analysis and showed that for larger sizes, the network is characterized by the apparition of spatiotemporally structured behavior, such as spiral waves or spatiotemporal chaos (see following sections).

From numerical simulations of Type 2 networks, a qualitatively similar behavior is observed. For small networks, the network displays a uniform periodic oscillation in which excitatory neurons oscillate in phase (Fig. 2). This oscillation is always present for networks of small sizes. Similar to Type 1 networks, this periodic oscillation was found to lose stability for higher size networks ($N = 144$ and $M = 36$) [30]. In the following section, we describe spatiotemporal solutions appearing in networks of larger size.

C. Intermittentlike behavior

As Ω_1 exceeds some critical value Ω_1^I, the stability analysis (for Type 1 connectivity) and numerical simulations show that periodic and stationary uniform solutions are unstable. As no other uniform solution exists, the system must necessarily adopt a nonuniform solution. Close to this critical value Ω_1^I, numerical simulation shows intermittentlike behavior (Fig. 4). Periods of uniform oscillatory regime alternate with periods of a more complex oscillatory behavior. A phase portrait shows that trajectories follow closely the uniform limit cycle, and make frequent "excursions" into another region of phase space before returning in the vicinity of the uniform solution.

Figure 4 also shows that the more complex oscillatory regime is characterized by a spatially nonuniform pattern of oscillations. In the following section, these nonuniform patterns are investigated in more detail.

Very close to the critical point Ω_1^I, the dynamics is largely dominated by the uniform oscillatory regime,

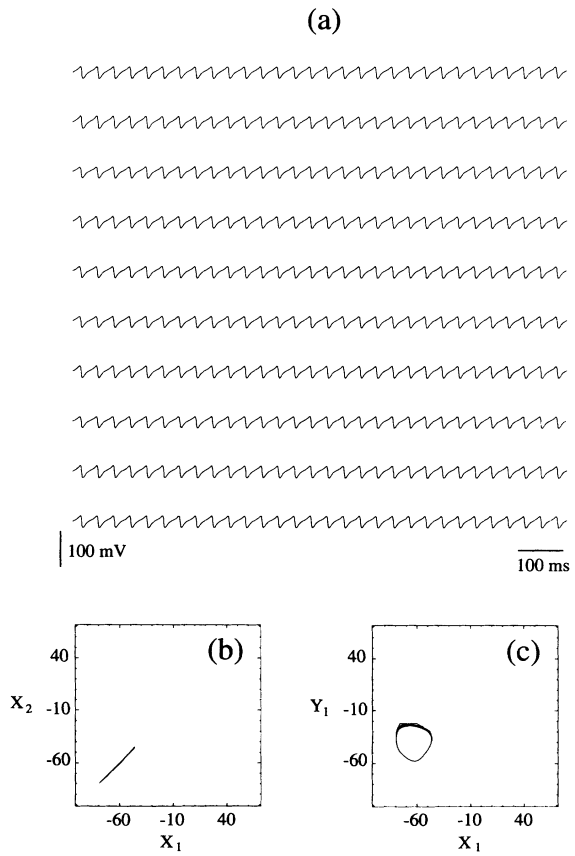

FIG. 2. Synchronized oscillation in the network. (a) Activity of ten excitatory cells randomly chosen in the network. (b) Phase portrait between two excitatory cells (X_1 and X_2). (c) Phase portrait between a pair of excitatory and inhibitory cells (X_1 and Y_1). Type 2 connectivity with $N = 100$, $M = 25$, and nearest-neighbor connections. $\Omega_1 = 14.25$, $\Omega_2 = \Omega_3 = 12.5$, and $\Omega_4 = 0$.

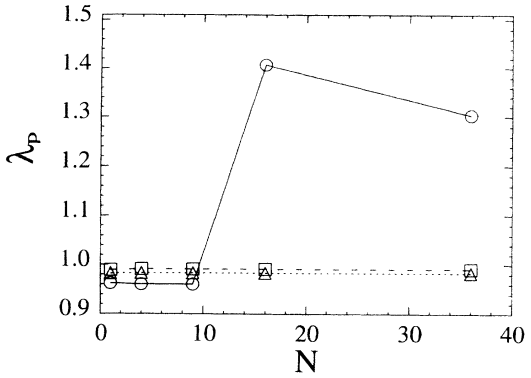

FIG. 3. Instability of the uniform periodic oscillations as a function of the size of the network. λ_P is the maximal eigenvalue of the evolution matrix of the system after discretization. λ_P is represented as a function of N for three values of excitatory synaptic weights $\Omega_1 = 12.565$ (squares, dashed lines), $\Omega_1 = 13.91$ (triangles, dotted lines), and $\Omega_1 = 15.27$ (circles, continuous lines). For $\Omega_1 = 12.565$ and $\Omega_1 = 13.91$, λ_P remains lower than unity and the uniform periodic solution is stable for all sizes considered. For $\Omega_1 = 15.27$, the uniform periodic solution is stable for small networks ($\lambda_P < 1$ for $N \leq 9$) and loses stability for larger networks ($\lambda_P > 1$ for $N > 9$). This stability analysis was performed for Type 1 networks with nearest-neighbor connections, $\Omega_2 = \Omega_3 = 12.5$ and $\Omega_4 = 0$. Modified from Ref. [25].

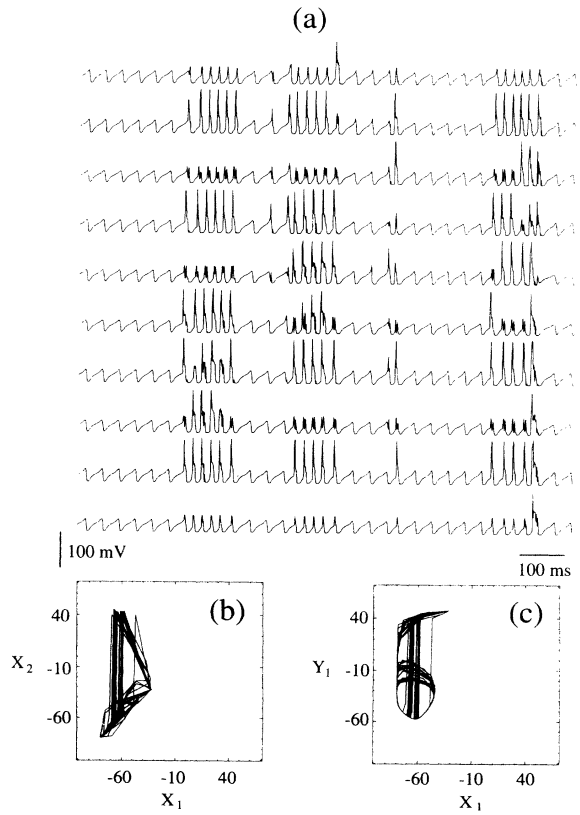

FIG. 4. Intermittentlike behavior of the network. (a) Activity of ten excitatory neurons. (b) Phase portrait between two excitatory cells (X_1 and X_2). (c) Phase portrait between a pair of excitatory and inhibitory cells (X_1 and Y_1). Parameters are identical to Fig. 2 with $\Omega_1 = 14.4$. The dynamics alternates between a quasiuniform oscillation and brief excursions to other regions of phase space.

making rare excursions into more complex oscillatory behavior. For increasing values of $\Omega_1 \geq \Omega_1^I$, periods of uniform oscillatory regime become less and less prominent. There exists a critical value Ω_1^T for which the uniform oscillation does not appear anymore. In this case, the system displays a nonuniform behavior which can be periodic or irregular, depending on the size of the system. These nonuniform solutions are described in the following sections.

D. Spiral and rotating waves

For moderate sizes of the system ($N \sim 100$), and for $\Omega_1 \geq \Omega_1^T$, stable rotating and spiral waves were observed for both types of architecture (Fig. 5). In this case, the trajectories converge towards a limit cycle which is different from the uniform limit cycle [Figs. 5(b) and 5(c)]. This nonuniform limit cycle is in a region of phase space which seems to correspond to the excursions of intermittentlike behavior (see preceding section).

The spatial portrait of spiral and rotating waves is a depolarizing wave of activity, which propagates in a rotat-

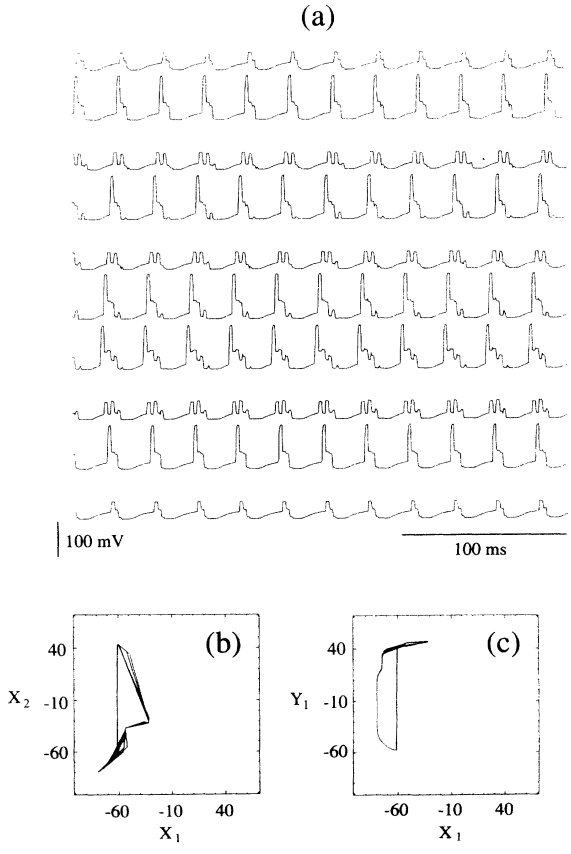

FIG. 5. Cellular activity during rotating or spiral waves. (a) Activity of 10 excitatory neurons. (b) Phase portrait between two excitatory cells (X_1 and X_2). (c) Phase portrait between a pair of excitatory and inhibitory cells (X_1 and Y_1). Parameters are identical to Fig. 2 with $\Omega_1 = 15$. The rotating wave corresponds to a nonuniform periodic solution as shown by the phase portraits.

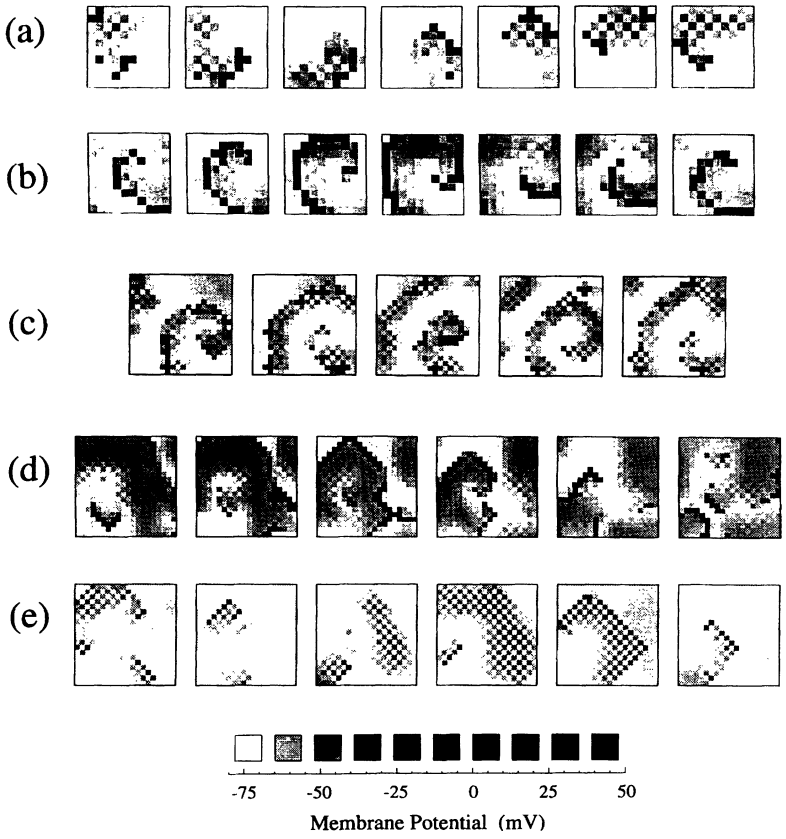

FIG. 6. Complex spatiotemporal patterns in $N = 100$ and $N = 400$ networks. Successive frames represent snapshots of the activity of the system taken at fixed time intervals. For each frame, only the activity of excitatory neurons is represented as a two-dimensional array of shaded squares. The value of the membrane potential for each neuron is shown as a gray scale ranging in ten steps from -75 mV (white) to 50 mV (black). (a), (b) Rotating spiral waves with a period of approximately 25 ms (4 ms between frames). Type 2 (a) and Type 1 (b) networks with $N = 100$ and nearest-neighbor connections. (c) Transient spiral wave (10 ms between frames). Type 2 network with $N = 400$ and nearest-neighbor connections. (d), (e) Spatiotemporal chaos (10 ms between frames). Type 1 (d) and Type 2 (e) networks with $N = 400$ and secondary-neighbor connectivity. All simulations were done with $\Omega_1 = 15$, $\Omega_2 = \Omega_3 = 12.5$, and $\Omega_4 = 0$.

ing fashion, with a period close to 25 ms [Figs. 6(a) and 6(b)]. In the vicinity of the depolarizing front, some cells are moderately depolarized while others are hyperpolarized. For Type 2 connectivity, it is frequent to observe a "checkerboard" pattern of activity, in which neighboring cells are in opposition of phase.

The rotating direction of the spiral wave entirely depends on the initial conditions, with an equal probability for both possible directions. There exists at least two coexisting stable limit cycles associated with spiral waves.

For larger sizes of the network (from $N \sim 400$), spiral waves appear transiently [Fig. 6(c)] but were never observed as a stable phenomenon. For example, for Type 2 connectivity with $N = 400$ and nearest-neighbor connections, no stable spiral wave could be observed, even though multiple initial conditions were used. In this case, the system behaves irregularly both in space and in time. Such irregular solutions are described in the following section.

E. Spatiotemporal chaos

Irregular spatiotemporal activity occurs for networks of both architectures and for relatively large sizes. This type of spatiotemporal chaotic activity is characterized by a multitude of depolarizing fronts that propagate in all directions and in an apparently disordered fashion [Figs. 6(d), 6(e), and 7(b)]. These excitation waves collapse with each other while new waves are spontaneously appearing. This chaotic type of activity is also seen at the cellular level at which individual neurons behave aperiodically [Fig. 7(a)]. These patterns are reminiscent of those seen in chemical turbulence [compare Fig. 7(b) with patterns seen in Ref. [31]].

The spatiotemporal dynamics of a larger size network are quite similar to smaller sizes with the same architecture [compare Fig. 6(e) with Fig. 7]. Depolarizing fronts are of comparable size. On the other hand, the architecture of the network seems to play a more determinant role on the type of patterns seen [compare Fig. 6(d) with Fig. 6(e)].

Phase portraits of spatiotemporal chaos show trajectories in a region of phase space which seems close to that of spiral waves [compare Figs. 5(b) and 5(c) with Fig. 8]. However, in this case, the trajectories are very irregular although they were similar for different network sizes (Fig. 8).

III. CHARACTERIZATION OF SPATIOTEMPORAL CHAOS

In this section, the loss of correlation with distance and the existence of a positive Lyapunov exponent are shown for the spatiotemporally chaotic solutions of Type 2 networks. The properties of information transport are also used to compare the uniform oscillation with more complex spatiotemporal dynamics.

A. Loss of correlation with distance

Figure 7(a) shows that neighboring cells are relatively correlated while randomly chosen cells seem to behave independently. Two methods are applied for quantifying this loss of correlation. First, the cross correlation function $C_{XY}(\tau)$ between two variables X and Y can be written as

$$C_{XY}(\tau) = \frac{\int (X(t) - \langle X \rangle)\ (Y(t+\tau) - \langle Y \rangle)\ dt}{\int (X(t) - \langle X \rangle)^2\ dt}, \quad (4)$$

where $\langle X \rangle$ and $\langle Y \rangle$ are the average values for X and Y, respectively.

Second, the time-delayed mutual information between these two variables can be defined as [32]

$$I_{XY}(\tau) = \int P(x,y,\tau)\ \log_2 \frac{P(x,y,\tau)}{P(x)\ P(y)}\ dx\, dy, \quad (5)$$

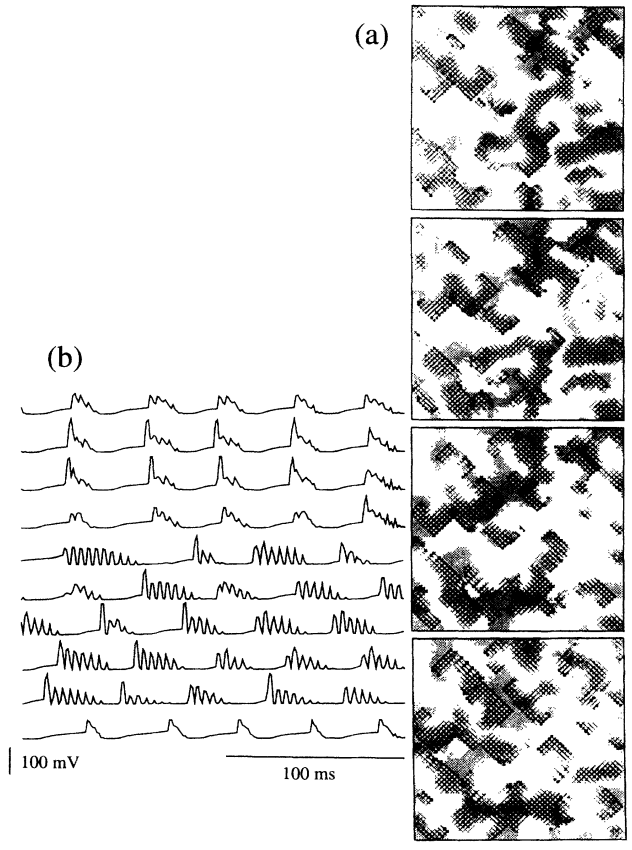

FIG. 7. Spatiotemporal chaos in a $N = 6400$ network. (a) Membrane potential of ten excitatory neurons. From top to bottom: four neighboring neurons and six randomly chosen neurons. (b) Snapshots of activity of the system (16 ms between frames from top to bottom). Type 2 secondary-neighbor connections with $N = 6400$, $M = 1600$, $\Omega_1 = 15$, $\Omega_2 = \Omega_3 = 12.5$, and $\Omega_4 = 0$. Numerous depolarizing waves are propagating in all directions, giving rise to an irregular dynamics.

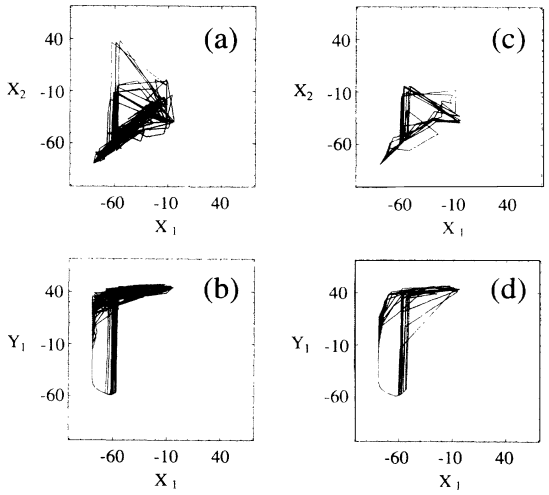

FIG. 8. Phase portraits during irregular spatiotemporal behavior. Two excitatory cells, X_1 and X_2, are represented in (a) and (c). An excitatory and an inhibitory cell, X_1 and Y_1, are displayed in (b) and (d). Type 2 networks were simulated with $N = 400$, $M = 100$ for (a) and (b), and $N = 6400$, $M = 1600$ for (c) and (d). Secondary-neighbor connectivity with $\Omega_1 = 15$, $\Omega_2 = \Omega_3 = 12.5$, and $\Omega_4 = 0$.

where $P(x)$ and $P(y)$ are the probability of observing the values $X = x$ and $Y = y$ independently. $P(x,y,\tau)$ is the joint probability of observing the values $X(t) = x$ and $Y(t+\tau) = y$ conjointly. If the logarithm is expressed in base 2, then $I_{XY}(\tau)$ is in units of bits.

These two functions were evaluated from the network with $N = 6400$ and $M = 1600$ and are displayed in Fig. 9. The loss of correlation appears strikingly when two neighboring cells are compared to two distant cells in the network. The cross correlation and the mutual information between two neurons vanish progressively as the distance between these neurons increases.

B. Largest positive Lyapunov exponent

The transition to spatiotemporal chaos strongly depends on the size of the system as well as its connectivity. In general, the simulations showed that there exists a critical size at which spatiotemporal chaos appears. This critical size depends on the connectivity and the architecture of the network. When the connectivity is increased, this critical size also increases.

The distinction between periodic phenomena, such as uniform oscillations, and irregular phenomena, such as spatiotemporal chaos, can be based on the estimation of the largest Lyapunov exponent. For a network of N variables X_i, $i = 1, ..., N$, the largest Lyapunov exponent can be defined as follows. Let $X_i(0)$ be an initial condition of the system, and $X_i'(0)$ another initial condition, very close to $X_i(0)$, such as the distance $\epsilon(0) = \sum_i (X_i(0) - X_i'(0))^2 << 1$. If the system is characterized by spatiotemporal chaos, then the distance be-

tween these two conditions is expected to increase exponentially. Therefore, the largest Lyapunov exponent [33] is defined by

$$\lambda = \lim_{t\to\infty} \frac{1}{t} \ln \frac{\epsilon(t)}{\epsilon(0)} = \lim_{t\to\infty} \frac{1}{t} \ln \frac{\sum_i (X_i(t) - X_i'(t))^2}{\sum_i (X_i(0) - X_i'(0))^2}. \quad (6)$$

We verified that this distance increased exponentially. A positive value of the exponent λ was estimated from the relation above, and was found to be insensitive to the particular initial condition chosen. Figure 10 summarizes the values obtained for different sizes and connectivities. At the critical size, λ jumps to a positive value. This critical size was estimated as $N = 144$ for nearest-neighbor connections, and $N = 400$ for secondary-neighbor. For denser connectivities, we could not observe any spatiotemporally chaotic behavior for $N \leq 6400$.

An important property is to be mentioned here. During spatiotemporal chaos, the distance $\epsilon(t)$ increases exponentially over a relatively long time. During stable uniform oscillations, $\epsilon(t)$ decreases and attains an approximately constant value after a few periods of the oscillation. This is the expected behavior during a convergence to a limit cycle. However, $\epsilon(t)$ has a more interesting behavior in the case of spiral waves. $\epsilon(t)$ increases exponentially during a few periods of the oscillation, then saturates at some ceiling level, giving a null Lyapunov exponent. The initial exponential increase corresponds to irregular transients, and the saturation occurs when the spiral wave stabilizes. Interestingly, the Lyapunov exponent during these transients is of the same order as that evaluated during spatiotemporal chaos.

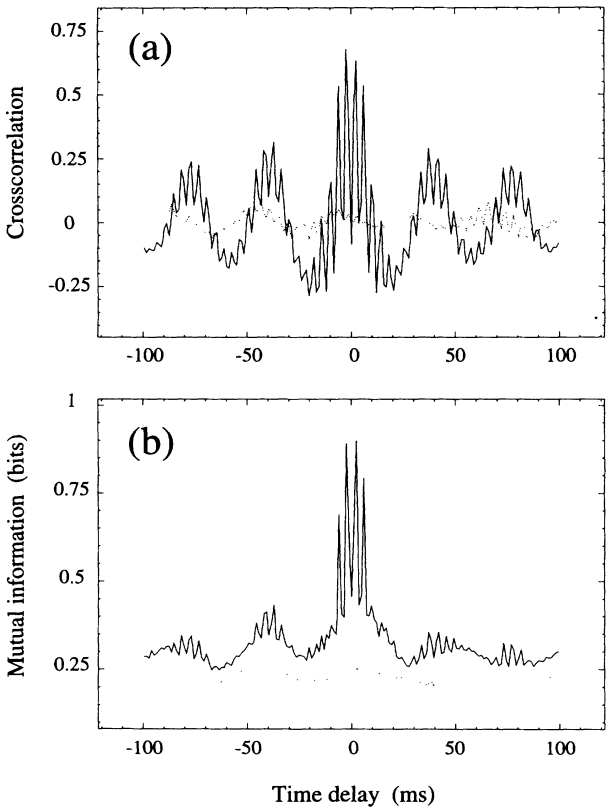

FIG. 9. Loss of correlation with distance during irregular spatiotemporal behavior. (a) Cross correlation and (b) mutual information. These functions evaluated for two neighboring excitatory cells (X_{85}, X_{86}) are represented by continuous lines. The values obtained from two excitatory cells separated by 16 intercellular distances (X_{85}, X_{335}) are shown by dotted lines. A total time of 10800 ms was simulated using a $N = 400$ and $M = 100$ Type 2 network with secondary-neighbor connections and with $\Omega_1 = 15$, $\Omega_2 = \Omega_3 = 12.5$, and $\Omega_4 = 0$. The mutual information was evaluated using an algorithm developed by Fraser and Swinney [32].

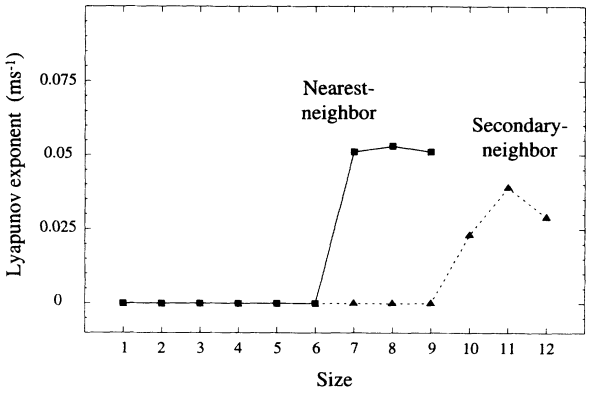

FIG. 10. Largest Lyapunov exponent as a function of the size of the network. The exponent (λ) is represented as a function of $\sqrt{N}/2$ for Type 2 networks ($M = N/4$, $\Omega_1 = 15$, $\Omega_2 = \Omega_3 = 12.5$, and $\Omega_4 = 0$). The exponent was calculated for networks with nearest-neighbor connections (squares) and secondary-neighbor connections (triangles). For small sizes, only periodic solutions are observed and the resulting exponent is zero. Spatiotemporal chaos is seen for higher sizes (positive values of λ).

C. Information transport

In this section, we estimate the information transport properties of a Type 2 network, following a method developed by Vastano and Swinney [34]. Vastano and Swinney considered a one-dimensional chain of coupled oscillators, in which every element was constituted by three nonlinear differential equations in limit cycle conditions, except for some oscillators which were in chaotic conditions. They showed that the spatial propagation phenomena in this system have analogies with a diffusion equation for mutual information. Similar considerations were also applied for other systems with coupled oscillators [35] or logistic maps [36].

We consider here the case of a $N = 100$ and $M = 25$ Type 2 network submitted to an irregular input, and we compare the behavior of the network during uniform oscillations and spatiotemporally more complex behavior. A reference neuron is submitted to a chaotic input provided by the Lorenz model [37]:

$$\begin{aligned} \frac{1}{c}\frac{dx}{dt} &= Pr\ (y-x), \\ \frac{1}{c}\frac{dy}{dt} &= r\ x - y - x\ z, \\ \frac{1}{c}\frac{dz}{dt} &= x\ y - b\ z, \end{aligned} \tag{7}$$

where $Pr = 10$, $b = 8/3$, $r = 28$, and $c = 0.03$. The equation for the membrane potential of the reference neuron, X_{ref}, possesses a supplementary term:

$$\frac{dX_{ref}}{dt} =, \cdots, -15\ (X_{ref} - E_1)\ g(z). \tag{8}$$

Here, the z variable of the Lorenz model is coupled to the reference neuron using the transfer function:

$$g(z) = 1/\left[1 + \exp\left(-0.65\ z + 15\right)\right].$$

This is equivalent to a chaotic synaptic drive on the reference neuron.

Figure 11 shows the mutual information measured between the reference neuron and other neurons located at increasing distances. The increasing time delay at which the mutual information peaks indicates the propagation of a wave of activity on the network, similar to the Vastano and Swinney case [34]. The position of the peak of mutual information, τ^*, is represented as a function of the distance, ρ, in Fig. 12(a) and is shown to increase linearly with distance. Similar results were obtained for different directions in the network. Thus there are concentric waves of activity, or target waves, that propagate from the reference cell at a constant velocity, v, which can be estimated from the slope of the curve in Fig. 12(a). The velocity for a network in stable resting state ($\Omega_1 < 12.1$) is approximatively identical to that during uniform periodic conditions ($12.1 < \Omega_1 < 14.35$), but decreases slightly during the spatiotemporal phase [$\Omega_1 > 14.35$, Fig. 12(b)].

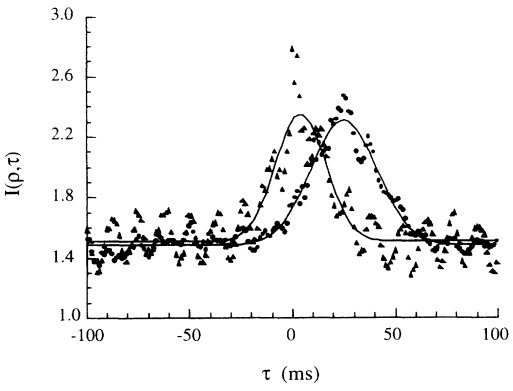

FIG. 11. Mutual information during chaotic forcing of the network. The mutual information $I(\rho, \tau)$ is calculated between a reference neuron (X_1) and other neurons at increasing distances (ρ). $\rho = 3$ (triangles) and $\rho = 9$ (circles) intercellular distances are shown here. A peak for a time delay of τ^* indicates the maximum of the wave of activity that propagated from the reference neuron. Continuous curves indicate the best fit of a normal distribution to these data. $N = 400$ Type 2 network with secondary-neighbor connectivity [same parameters as in Fig. 6(e)].

As pointed out by Vastano and Swinney [34], information transport can be defined if the mutual information $I(\rho, \tau)$ is assumed to be described as a normal distribution whose variance increases linearly with distance. In this case, $I(\rho, \tau)$ is the solution of a diffusion equation.

In the present case, we assume that there is a normal component in $I(\rho, \tau)$ due to the propagating waves emanating from the cell submitted to the external input. In addition to this normal component, there are also other components similar to Fig. 9(b), due to the spontaneous activity of the network. This is also indicated by the vanishing of the latter components for larger distances ρ (circles in Fig. 11). From Fig. 11, it can also be seen that the width of the mutual information peak increases in function of the distance. As in the Vastano-Swinney case, the variance of the peak, σ^2, increases linearly with the distance ρ [Fig. 13(a)].

We therefore provided a direct fit of $I(\rho, \tau)$ using a normal distribution whose variance increases linearly with distance, such as

$$I(\rho, \tau) \sim \exp\left[-\frac{(\tau - \tau^*)^2}{4D_0\rho}\right], \tag{9}$$

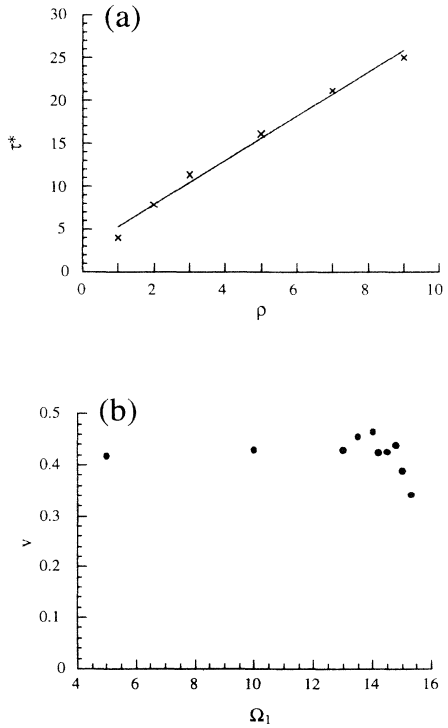

FIG. 12. Information transport in the network. (a) Position of the maximum τ^* of the mutual information as a function of distance ρ (in units of intercellular distances). The linear relation indicates that the peak of mutual information propagates with a constant velocity. The straight line shows a linear regression, where the slope gives the inverse of the velocity. (b) Velocity v, as estimated from (a), as a function of the synaptic weight Ω_1. The velocity is expressed in units of intercellular distance per ms.

where D_0 is a positive constant.

Through the change of variables $r = v\tau$ and $t = \rho/v$, one obtains

$$I(r,t) \sim \exp\left[-\frac{(r-r^*)^2}{4Dt}\right], \tag{10}$$

where $D = D_0 v^3$. This expression corresponds to the solution of a diffusion equation:

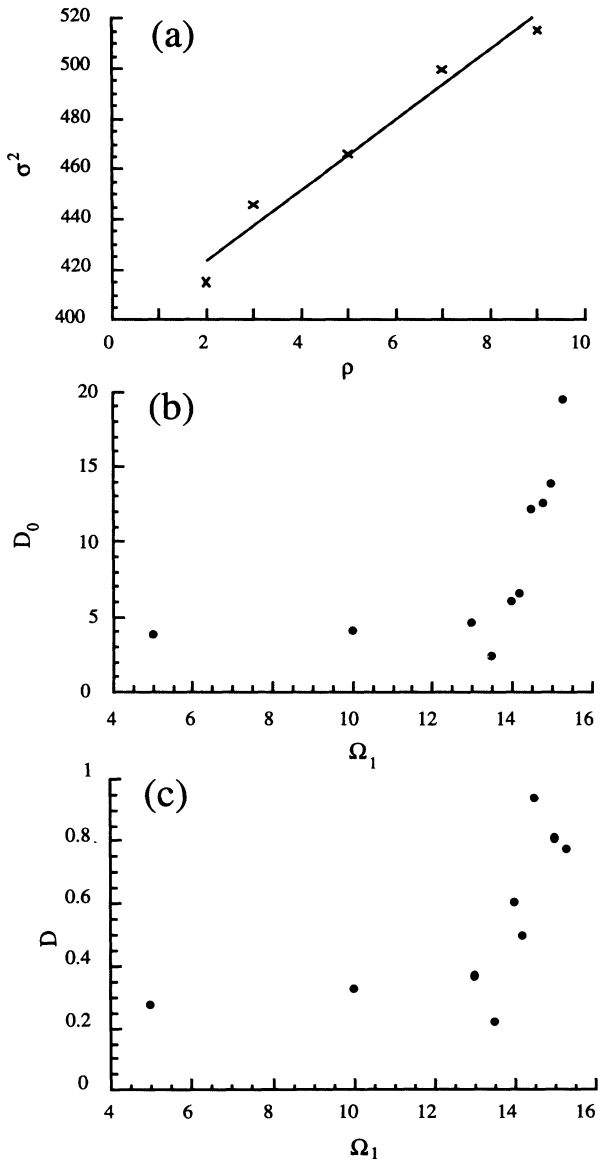

FIG. 13. Transport coefficients of mutual information. (a) Variance of the peak of mutual information, σ^2, as a function of the distance in the network, ρ. There is a linear increase of σ^2 with ρ, and the straight line represents a linear regression, where the slope is the information transport coefficient D_0. (b) Information transport coefficient D_0 as a function of synaptic weight Ω_1. D_0 is expressed in units of ms^2 (intercellular distance)$^{-1}$. (c) Diffusion coefficient of information. The diffusion coefficient D is represented as a function of Ω_1. In (b) and (c), transport coefficients reach the highest values during spatiotemporal chaos.

$$\frac{\partial I}{\partial t} = D\,\frac{\partial^2 I}{\partial r^2}. \tag{11}$$

Here, D is the diffusion coefficient of mutual information.

The change of variable made in Eq. (10) corresponds to the measurement of the mutual information relative to the peak of the wave of activity. Equation (11) therefore describes the broadening of the mutual information by a diffusion process.

The components of $I(\rho,\tau)$ due to the spontaneous activity induce some error in the estimation of information transport properties, but nevertheless the diffusion coefficient D could be estimated reliably [38]. D was evaluated following a similar procedure for various values of the parameters. Figures 13(b) and 13(c) illustrate the dependency between the transport coefficients D_0 and D, and the synaptic weight Ω_1. The transport coefficients remain approximately constant when the network shows a stable resting state or uniform periodic oscillations. On the other hand, there is a sensible increase of D_0 and D when the network displays more complex spatiotemporal behavior. The same procedure was applied to a Type 1 network with $N = 100$ for two values of Ω_1. There was also a sensible increase of D in the spatiotemporal phase.

DISCUSSION

Oscillatory activity in networks of excitatory and inhibitory neurons can arise from two basic mechanisms. First, neurons can be provided with the appropriate set of intrinsic voltage-dependent conductances (see Ref. [9]) that allows the membrane potential to oscillate. Second, the highly nonlinear synaptic interactions may induce oscillations in otherwise quiescent neurons. Numerous experimental evidence indicate that both intrinsic and synaptic properties play a role in the genesis of these oscillatory phenomena [10].

In this paper, we have addressed the problem of the genesis of oscillatory and complex phenomena in two-dimensional networks of excitatory and inhibitory neurons. In order to keep "minimal" conditions for generating these spatiotemporal behaviors, both intrinsic properties and connection architecture of the neurons were reduced to the simplest cases. We discuss here the properties of the complex spatiotemporal behavior of these networks as well as possible biological predictions or experimental applications.

Properties of complex spatiotemporal phenomena

The set of equations used is perfectly isotropic; all neurons connect their neighbors with the same pattern of connectivity, and with the same values of the synaptic weights. Although the membrane equations for single neurons were reduced to an extremely simple form, the network could still display very complex behavior. The use of isotropic networks is revealed as an extremely useful approach that allowed us to determine some important properties of the network behavior.

The relatively simple architecture of the network allowed us to estimate the importance of various parameters in generating oscillatory and complex phenomena. The first factor is the locality of the connectivity. Local connection patterns are essential here for generating spatiotemporal phenomena. In general, increasing the extent of the connectivity results in more stable uniform oscillations (see Fig. 10), but if the size of the network is taken large enough, similar instabilities as described above are seen. Another extremely important parameter is the time delay. None of the complex spatiotemporal phenomena described here could be observed with zero time delay. However, the dynamical behavior exhibited by the network is relatively insensitive to the value of the delay, provided it is taken in a reasonable range. In the range of delays of about 1 to 5 ms, the network behaves qualitatively the same, but the precise position of the bifurcation points are affected by the value of the time delay. Finally, the synaptic weights are extremely critical too. The interconnections between excitatory and inhibitory neurons must be strong enough for the system to display oscillations [16,24]. In these conditions, excitatory to excitatory interconnections, with corresponding weight Ω_1, determine the transitions.

The particular role of the size of the network (the number of neurons) is particularly apparent in this model because of its simple architecture. The absence of irregularity in the connection patterns, and the identity of the connectivity across different sizes, allows us to consider the size of the network as a particular parameter. Type 1 and Type 2 networks display a series of instabilities as the size is increased, leading to spatiotemporal chaos. In general, for a given size, there exists a range of values of Ω_1 for which uniform oscillations are stable. As the size is increased, this range narrows and spatiotemporal chaotic solutions becomes the most prominent behavior. In addition, the spatial patterns of spatiotemporal chaos display some similarities for different sizes [compare Fig. 6(e) with Fig. 7(b)]. The main difference is that for larger systems the same type of patterns develop in a larger two-dimensional space. These patterns apparently have characteristic length and time scales which are independent of the size of the network. Intuitively, this suggests that uniform oscillations are seen only for small networks because the size is too small to generate these patterns.

Comparison of the patterns displayed during spatiotemporal chaos in the network [Fig. 7(a)] with a previous study [24] suggests a possible involvement of homoclinic phenomena. Scrutiny of the traces of excitatory neurons in Fig. 7(a) reveals that most neurons display bursting oscillations. In a previous study [24], we showed in the same model that bursting oscillations occur following a homoclinic tangency to an unstable limit cycle. The period and the amplitude of these bursting oscillations are very similar to those observed during spatiotemporal chaos, therefore suggesting that homoclinic phenomena are involved in this type of spatiotemporally complex dynamics, but further investigation would be needed to demonstrate this point.

Although the present model is more complex than other solvable models (see for example Refs. [17,39,40]), it nevertheless allowed us to investigate the bifurcations underlying oscillations and spatiotemporal chaos. The system was first studied with $N = M = 1$ [24] and the bifurcation diagram obtained was very similar as larger systems. In the case of networks with $N, M > 1$, stability analysis could be performed for the fixed points [16,23,28] and the uniform periodic solutions [25]. The stability of the fixed points was independent of the size of the system and the periodic solutions exist in the same range of Ω_1. However, in the network, if Ω_1 is increased over some critical value, the uniform periodic oscillation can become unstable, giving rise to complex spatiotemporal behavior. Both numerical simulations and stability analysis showed such an instability. Numerically, it was observed that the transition between uniform oscillations and spatiotemporal phenomena arises through intermittentlike behavior (Fig. 4). Further augmentation of Ω_1 leads to spatiotemporal chaos.

As a consequence of its simple architecture, it is easy to compare the present model with other studies of homogeneous networks of oscillators. Type 1 networks can be seen as networks of oscillators with excitatory connections. One of the most salient features of the present model is the instability of the uniform periodic oscillation as the sole factor of the size of the system is increased (continuous curve in Fig. 3). In comparison, networks of oscillators [31,41] also display an instability of the uniform oscillation, but in such a case, this instability arises from a change in the coupling between oscillators. However, in the present model, the uniform oscillation is always stable with all-to-all connectivity but unstable if connections are made locally, in accordance with some models [20,40] but in contrast to others [19].

Finally, isotropic networks are also well suited for investigating the decay of correlations, or for defining transport properties. The estimation of the mutual information and cross correlations showed a loss of correlation with distance during spatiotemporal chaos. Information transport [34] was defined by submitting one neuron in the network to an irregular input. It was found that if mutual information is assumed to obey a normal distribution, then the broadening of the waves of activity can be described by a diffusion equation. Interestingly, as the excitability of the system is enhanced, the diffusion coefficient increases and reaches the highest values during spatiotemporal chaos.

These properties are intriguingly similar to some aspects of fluid dynamics. Two of the main characteristics of fluid turbulence are the loss of correlation with distance and a significant increase in transport coefficients [42]. As these properties are also seen here qualitatively, it is therefore tempting to describe spatiotemporal chaos in a neural network as a form of "neuronal turbulence". In the same way that turbulence can be seen as a state which maximizes the transport of various quantities such as heat, matter, etc., it might be that in networks of neurons, spatiotemporal chaos is a state where the transport of information-related quantities is optimal. The transfer of activity between neurons is the highest during these complex dynamics, suggesting that

complex spatiotemporal behavior is seen for high values of excitatory weights because neurons naturally adopt a dynamical state in which the communication between cells is optimized.

An interesting issue is whether the increase of information transport during spatiotemporal chaos is specific to the present model or if it is a general property. In the latter case, the same property should be observed in other model systems, like the Ginzburg-Landau equations or chemical turbulence [31]. In principle, the same procedure as described here could be also realized experimentally in systems showing spatiotemporal chaos or turbulent phenomena (see discussion below).

Biological predictions

It is to be reminded that homogeneous and isotropic networks such as those studied here are certainly not biologically realistic. However, if one assumes that the properties found in the present model are generic and also found in systems with more complex architecture, such as the cerebral cortex, then the present results can suggest useful hypotheses or possible experimental verifications of the properties found here.

First, a study of networks of oscillators with all-to-all coupling [41] suggested that the behavior of firing rate-based models might be generic to more realistic spiking models. In particular, they showed that the longest wavelength modes of a spiking model match closely those of the firing rate analog of the same system. It is likely that the instability of the uniform oscillation shown here, and also observed in the network of oscillators [41], might also subsist in models based on a more realistic synaptic interaction, but further work is needed to demonstrate this point.

Second, by analogy with the model of Wilson and Cowan [15], the variables X_i and Y_i can be interpreted as the fraction of excitatory or inhibitory cells active per unit of time. The network could then be thought to represent a large array of interacting *populations* of neurons rather than a few tens of hundreds of cells. As anatomical data [26,43] show that inhibitory cells tend to send their connections vertically, in contrast with the longer range horizontal connectivity of some excitatory cells, Type 1 networks are a possible candidate for modeling populations of interacting cortical neurons. In this case, the present Type 1 model shows that large networks with isotropic architecture do not sustain synchronized rhythmicity, but rather show spatiotemporally complex phenomena. As this model did not take into account the intrinsic properties of cortical cells (reviewed in [44]), it might be that intrinsic properties could play a role in sustaining stable synchronized oscillations in large networks of excitatory and inhibitory neurons.

More realistic models should be drawn for addressing these questions, by incorporating the typical laminated structure of the cerebral cortex [26], the particular connectivity of each layer, the various types of cortical neurons, and their complex synaptic interactions and intrinsic properties [44].

Finally, as mentioned above, it is possible to provide experimental measurements from some of the properties that were estimated here. In particular, information transport could be investigated experimentally with a standard electrophysiological setup. An aperiodic electrical stimuli [such as $g(z)$ above] can be delivered through a stimulating extracellular microelectrode, and the activity can be recorded using two field potential electrodes; the first one is the reference electrode and stays very close to the stimulated site, and the second one is placed at increasing distances. If the stimulus gives rise to a measurable propagation of activity, then this setup should allow us to estimate information transport coefficients using similar procedures as described in this paper.

As different oscillatory states are seen in brain activity during sleep and wakefulness, it is unlikely that they are characterized by the same spatiotemporal properties, as indicated by the very different values of correlation dimension between wakefulness [5], sleep [3,6], or epileptic seizures [4]. The methods used here could therefore be useful to assess important properties of the spatiotemporal dynamics which might be complementary to those provided by time-series analysis.

ACKNOWLEDGMENTS

This research was partly supported by the Belgian Government (ARC and IMPULS, Project No. RFO AI 10), and by the E.E.C. (ESPRIT, Basic Research, Project No. 3234). I wish to acknowledge Dr. Agnessa Babloyantz, Dr. Pierre Gaspard, and Dr. Terrence Sejnowski for stimulating discussions and continuous support.

[1] W. Singer, Prog. Brain Res. **95**, 461 (1993).
[2] M. Steriade, E.G. Jones, and R.R. Llinas, *Thalamic Oscillations and Signalling* (John Wiley & Sons, New York, 1990).
[3] A. Babloyantz, C. Nicolis, and M. Salazar, Phys. Lett. A **111**, 152 (1985).
[4] A. Babloyantz and A. Destexhe, Proc. Natl. Acad. Sci. USA **83**, 3513 (1986).
[5] P.E. Rapp, T.R. Bashore, J.M. Martinerie, A.M. Albano, and I.D. Zimmerman, Brain Topogr. **2**, 99 (1989).
[6] J. Roschke and J. Aldenhoff, Biol. Cyber. **64**, 307 (1991).
[7] W. Softky and C. Koch, J. Neurosci. **13**, 334 (1993).
[8] H. Noda and W.R. Adey, Brain Res. **18**, 513 (1970).
[9] R.R. Llinas, Science **242**, 1654 (1988).
[10] M. Steriade, D.A. McCormick, and T.J. Sejnowski, Science **262**, 679 (1993); A. Destexhe, D. Contreras, T.J. Sejnowski, and M. Steriade, J. Neurophysiol. (to be published).
[11] X.J. Wang and J. Rinzel, Neural Comput. **4**, 84 (1992).
[12] A. Destexhe, D.A. McCormick, and T.J. Sejnowski, Biophys. J. **65**, 2474 (1993).
[13] M. Steriade and R.R. Llinas, Physiol. Rev. **68**, 649

(1988).
[14] M. von Krosigk, T. Bal, and D.A. McCormick, Science **261**, 361 (1993).
[15] H.R. Wilson and J.D. Cowan, Kybernetik **13**, 55 (1973).
[16] L.K. Kaczmarek, Biol. Cyber. **22**, 229 (1976).
[17] A. Atiya and P. Baldi, Int. J. Neural Syst. **1**, 103 (1989).
[18] A. Destexhe and A. Babloyantz, Neural Comput. **3**, 145 (1991).
[19] P. Konig and T.B. Schillen, Neural Comput. **3**, 155 (1991); T.B. Schillen and P. Konig, *ibid.* **3**, 167 (1991).
[20] G.B. Ermentrout, SIAM J. Appl. Math. **52**, 1665 (1992).
[21] E.R. Kandel and J.H. Schwartz, *Principles of Neural Science* (Elsevier, Amsterdam, 1985).
[22] S. Grossberg, *The Adaptive Brain* (North-Holland, Amsterdam, 1987).
[23] L.K. Kaczmarek and A. Babloyantz, Biol. Cyber. **26**, 199 (1977).
[24] A. Destexhe and P. Gaspard, Phys. Lett. A **173**, 386 (1993).
[25] A. Destexhe, Phys. Lett. A **187**, 309 (1994).
[26] *Cerebral Cortex*, edited by E.G. Jones and A. Peters (Plenum Press, New York, 1984).
[27] V. Braitenberg, in *Brain Theory*, edited by G. Palm and A. Aertsen (Springer, Berlin, 1986).
[28] A. Destexhe, Ph.D. dissertation, Université Libre de Bruxelles, Brussels, 1992.
[29] Stability analysis of the fixed points of both types of architecture was performed [28] by using a method specific to delay equations introduced by C.M. Marcus and R.M. Westervelt, Phys. Rev. A **39**, 347 (1989).
[30] The same stability analysis as described in Ref. [25] was performed for Type 2 networks. It was found that the uniform periodic solution is stable up to $N = 36$ and $M = 9$. Stability analysis of larger systems would require very large computer memory and could not be performed for this reason.
[31] Y. Kuramoto, *Chemical Oscillations, Waves and Turbulence* (Springer, Berlin, 1984).
[32] A.M. Fraser and H.L. Swinney, Phys. Rev. A **33**, 1134 (1986).
[33] The exponent calculated using Eq. (6) is only an approximation of the largest Lyapunov exponent since a delay equation is infinite-dimensional. However, the positivity of this exponent is sufficient to prove the exponential divergence of the trajectories.
[34] J.A. Vastano and H.L. Swinney, Phys. Rev. Lett. **60**, 1773 (1988).
[35] K. Matsumoto and I. Tsuda, J. Phys. A **21**, 1405 (1988).
[36] K. Kaneko, Physica D **23**, 436 (1986).
[37] E.N. Lorenz, J. Atmos. Sci. **20**, 130 (1963).
[38] Very similar values of the variance are obtained if the components due to the spontaneous activity [as in Fig. 9(b)] are substracted from the mutual information obtained in Fig. 11. Therefore, it is assumed that the effect of these components on the diffusion coefficient is small.
[39] H. Sompolinsky, D. Golomb, and D. Kleinfeld, Phys. Rev. A **43**, 6990 (1991).
[40] D. Hansel and G. Mato, Physica A **200**, 662 (1993).
[41] L.F. Abbott and C. van Vreeswijk, Phys. Rev. E **48**, 1483 (1993).
[42] A.S. Monin and A.M. Yaglom, *Statistical Fluid Mechanics. Mechanics of Turbulence* (MIT Press, Cambridge, MA, 1971).
[43] P. Somogyi, A. Cowey, N. Halasz, and T.F. Freund, Nature (London) **294**, 761 (1981).
[44] B.W. Connors and M.J. Gutnick, Trends Neurosci. **13**, 99 (1990).

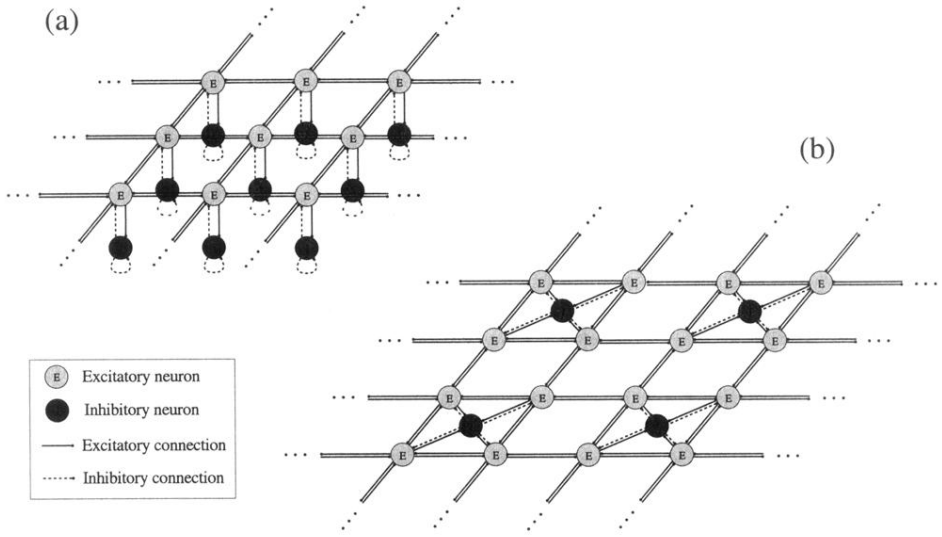

FIG. 1. Two different types of architecture of a network of excitatory and inhibitory neurons. For each type of architecture a few neurons are represented to illustrate the connectivity. Neurons are symbolized by shaded circles and connections by straight lines (see legend). (a) Type 1 connectivity. The network consists of a series of pairs of excitatory and inhibitory neurons arranged on a two-dimensional lattice. Connections between adjacent pairs are made between excitatory neurons only. (b) Type 2 connectivity. Excitatory and inhibitory neurons are in the ratio of 75% to 25%, and are equally distributed on the two dimensional network. For each type of architecture, only nearest-neighbor connections have been represented for simplicity.

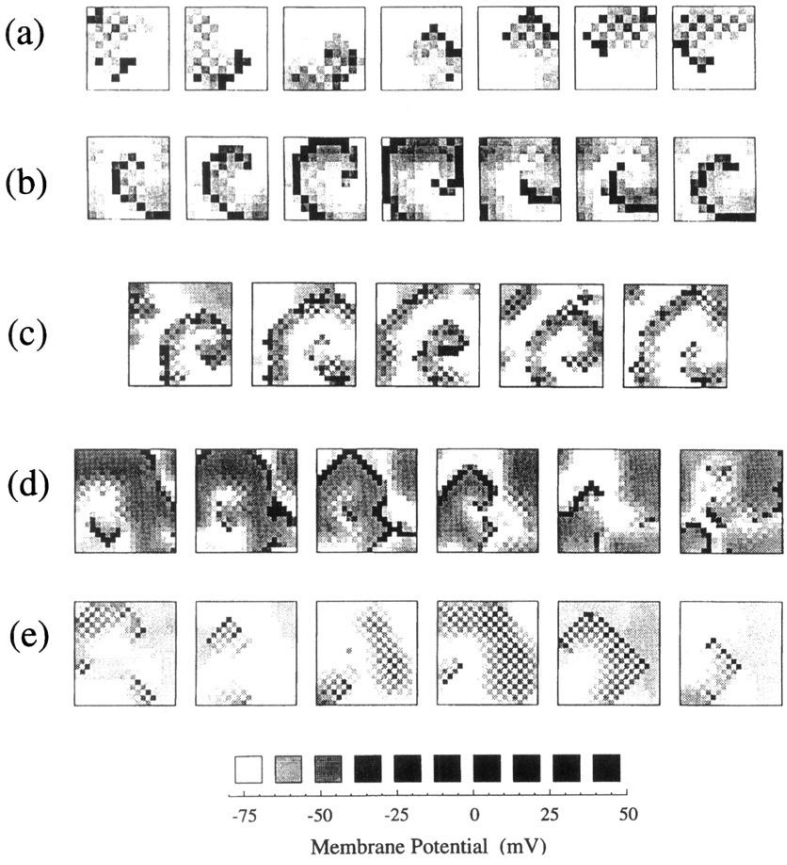

FIG. 6. Complex spatiotemporal patterns in $N = 100$ and $N = 400$ networks. Successive frames represent snapshots of the activity of the system taken at fixed time intervals. For each frame, only the activity of excitatory neurons is represented as a two-dimensional array of shaded squares. The value of the membrane potential for each neuron is shown as a gray scale ranging in ten steps from -75 mV (white) to 50 mV (black). (a), (b) Rotating spiral waves with a period of approximately 25 ms (4 ms between frames). Type 2 (a) and Type 1 (b) networks with $N = 100$ and nearest-neighbor connections. (c) Transient spiral wave (10 ms between frames). Type 2 network with $N = 400$ and nearest-neighbor connections. (d), (e) Spatiotemporal chaos (10 ms between frames). Type 1 (d) and Type 2 (e) networks with $N = 400$ and secondary-neighbor connectivity. All simulations were done with $\Omega_1 = 15$, $\Omega_2 = \Omega_3 = 12.5$, and $\Omega_4 = 0$.

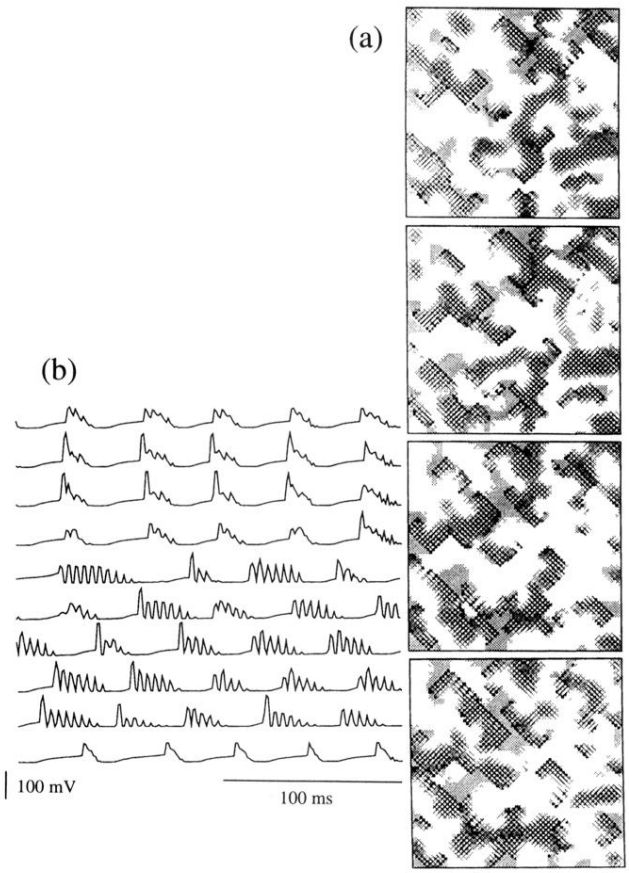

FIG. 7. Spatiotemporal chaos in a $N = 6400$ network. (a) Membrane potential of ten excitatory neurons. From top to bottom: four neighboring neurons and six randomly chosen neurons. (b) Snapshots of activity of the system (16 ms between frames from top to bottom). Type 2 secondary-neighbor connections with $N = 6400$, $M = 1600$, $\Omega_1 = 15$, $\Omega_2 = \Omega_3 = 12.5$, and $\Omega_4 = 0$. Numerous depolarizing waves are propagating in all directions, giving rise to an irregular dynamics.